TopAwaRe: Topology-Aware Registration

Rune Kok Nielsen[1], Sune Darkner[1], and Aasa Feragen[1,2(✉)]

[1] Department of Computer Science, University of Copenhagen, Universitetsparken 5, 2100 Copenhagen, Denmark
{darkner,aasa}@di.ku.dk
[2] DTU Compute, Technical University of Denmark, Richard Petersens Plads 324, 2800 Kgs Lyngby, Denmark
afhar@dtu.dk

Abstract. Deformable registration, or nonlinear alignment of images, is a fundamental preprocessing tool in medical imaging. State-of-the-art algorithms restrict to diffeomorphisms to regularize an otherwise ill-posed problem. In particular, such models assume that a one-to-one matching exists between any pair of images. In a range of real-life-applications, however, one image may contain objects that another does not. In such cases, the one-to-one assumption is routinely accepted as unavoidable, leading to inaccurate preprocessing and, thus, inaccuracies in the subsequent analysis. We present a novel, piecewise-diffeomorphic deformation framework which models topological changes as explicitly encoded discontinuities in the deformation fields. We thus preserve the regularization properties of diffeomorphic models while locally avoiding their erroneous one-to-one assumption. The entire model is GPU-implemented, and validated on intersubject 3D registration of T1-weighted brain MRI. Qualitative and quantitative results show our ability to improve performance in pathological cases containing topological inconsistencies.

Keywords: Image registration · Diffeomorphisms · Topology-Aware

1 Introduction

Deformable image registration aims to align two images by non-linearly matching points between them, which is one of the most fundamental problems in medical imaging. Use cases include intra- and intersubject registration in e.g. longitudinal or population studies, respectively. To keep the optimization problem feasible, state-of-the-art registration frameworks limit themselves to *diffeomorphic* warps, which in particular assume a one-to-one mapping between the image domains. Real life is, however, rich with cases where one image contains matter that the other does not, thus violating the one-to-one assumption. Such pairs of images are *topologically different* in the sense that optimal alignment of the images requires tearing at least one of the image domains.

D. Shen et al. (Eds.): MICCAI 2019, LNCS 11765, pp. 364–372, 2019.
https://doi.org/10.1007/978-3-030-32245-8_41

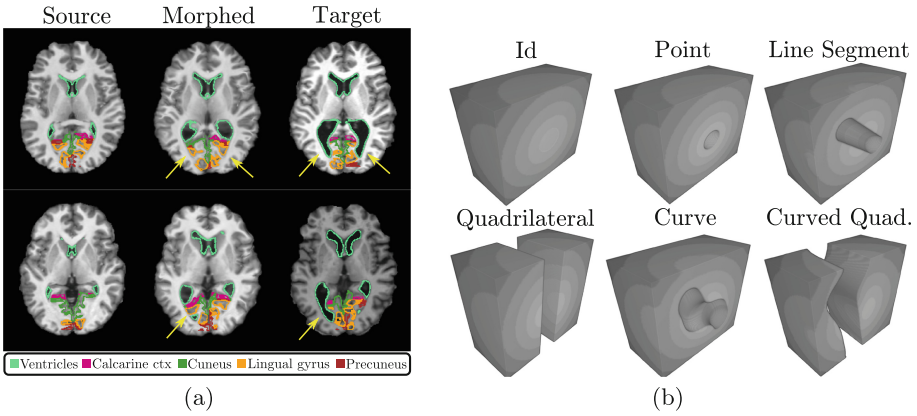

Fig. 1. (a): Diffeomorphic registration with ANTs [1] from sources with contracted ventricles to targets with expanded ventricles. The topological differences cause clear issues by the ventricles. (b) Toy example volume sliced in half following discontinuous deformation by various expansions using our deformation model.

We propose applying domain knowledge of the image topologies to handle topological changes during registration. We derive a novel framework for piecewise-diffeomorphic image registration, combining state-of-the-art diffeomorphic registration with a topology-altering model. The topology of the image domain is altered by expanding topological holes from predefined discontinuities in the form of points, curves or surfaces, as shown in Fig. 1(b). These *expansions* are simultaneously morphed into target shapes by a diffeomorphic model. We name this concept *Topology-Aware Registration* (TopAwaRe).

We validate the model on intersubject registration of T1-weighted brain MRI where some subjects have expanded ventricles in the back of the brain, which appears under pathological conditions including Alzheimer's disease. To motivate this challenge, consider the two examples in Fig. 1(a), where diffeomorphic registration locally fails due to the change of topology between source subjects with contracted ventricles and target subjects with expanded ventricles.

Related Work: Diffeomorphic registration methods [1,3] perform well when the diffeomorphic assumption is reasonable, but are in their nature unable to model discontinuities. The sliding motion between organs is a type of discontinuity that has received significant attention [5,9,10]. Other approaches to topological changes include individual parameterization of segmented organs [4] and supporting registration of pre-operative to post-recurrence scans of tumor patients by segmentation of pathological regions [6]. However, neither of these models support changing the topology within a connected region, nor modeling the interaction between an expanding hole and its surroundings. In recent years, deep learning models for registration have emerged [2]. However, these methods still optimize for global smoothness and do not account for topological changes.

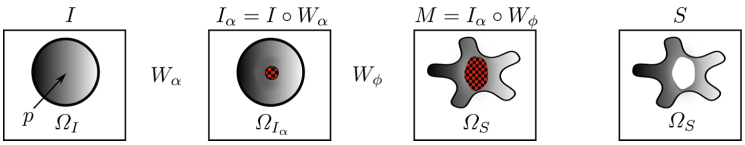

Fig. 2. Warp composition diagram: The source I is topologically altered by W_α expanding a spherical hole from p. The result I_α is morphed to match the target S.

2 Model

Deformable registration seeks the warp $W\colon \Omega_S \to \Omega_I$ aligning a source image $I\colon \Omega_I \to \mathbb{R}^d$ into the coordinate system of a target image $S\colon \Omega_S \to \mathbb{R}^d$. We denote the morphed image $M = I \circ W$, and W is then determined through an optimization process minimizing the combination $\mathcal{M}(S, I \circ W) + \mathcal{S}(W)$ of a matching term $\mathcal{M}$ and a regularization term $\mathcal{S}$ acting on the warp itself. The registration model controls a pull-back deformation vector field $u\colon \mathbb{R}^n \to \mathbb{R}^n$ such that $W = \mathrm{Id} - u$. In our proposed framework, the warp W is given by a composition $W = W_\alpha \circ W_\phi$ of respectively piecewise- and globally diffeomorphic warps W_α and W_ϕ (see Fig. 2). Here, W_α is controlled by a specialized topology-changing model and W_ϕ by a diffeomorphic registration model. The resulting W is piecewise-diffeomorphic with known discontinuities.

Topological differences are handled by inducing and expanding holes from predefined discontinuities, as illustrated in Fig. 2. The effects of an expansion are **(A)** discontinuous expansion in the deformation field and **(B)** changing intensity within the hole in the morphed image. This change of intensity is controlled through an alpha channel $\alpha\colon \Omega_S \to [0, 1]$ such that any $\boldsymbol{x} \in \Omega_S$ with $\alpha(\boldsymbol{x}) = 0$ is within a hole and $\alpha(\boldsymbol{x}) = 1$ is in the regular domain. We allow $0 < \alpha(\boldsymbol{x}) < 1$ to address partial volume effects near the boundaries. The morphed image then becomes a convex combination

$$M_\alpha(\boldsymbol{x}) = \alpha(\boldsymbol{x})M(\boldsymbol{x}) + (1 - \alpha(\boldsymbol{x}))\beta(\boldsymbol{x}), \tag{1}$$

where $\beta\colon \Omega_S \to \mathbb{R}^d$ decides within-hole intensity and thus affects optimization.

Expansions. We present the various types of expansions (illustrated in Fig. 1(b)) in order of increasing complexity following a common approach. We derive the case of single expansions as they are modeled individually and composed. As illustrated in Fig. 2, we introduce an intermediary domain Ω_{I_α} corresponding to the source image after being altered by the expansions, and specify $W_\alpha\colon \Omega_{I_\alpha} \to \Omega_I$ and $W_\phi\colon \Omega_S \to \Omega_{I_\alpha}$.

In radial expansion from a single point $\boldsymbol{p} \in \Omega_I$, the radius of the resulting sphere in Ω_{I_α} is denoted by Π and optimized during registration. As the sphere constitutes a hole, any point $\boldsymbol{x} \in \Omega_{I_\alpha}$ within it is considered as background, i.e. $\alpha(\boldsymbol{x}) = 0$. The deformation caused by the growth is designed to be isotropic at $\boldsymbol{p}$, decreasing in magnitude and have compact support. The

pull-back displacement u_α caused by the expansion is given by the directional vector $\frac{\overrightarrow{\boldsymbol{px}}}{||\overrightarrow{\boldsymbol{px}}||}$ scaled by a radial basis function (RBF) $s\colon \Omega_{I_\alpha} \to \mathbb{R}^+$, such that

$$u_\alpha(\boldsymbol{x}) = s(\boldsymbol{x})\frac{\overrightarrow{\boldsymbol{px}}}{||\overrightarrow{\boldsymbol{px}}||}. \tag{2}$$

The displacement magnitude s is affected by the radius Π and a smoothing parameter σ such that the reach of the displacement is exactly $(1+\sigma)\Pi$. In the pull-back mapping, any point within the sphere is sent to its center, giving

$$s(\boldsymbol{x}) = ||\overrightarrow{\boldsymbol{px}}|| \qquad \text{for } ||\overrightarrow{\boldsymbol{px}}|| \leq \Pi, \tag{3}$$

and any point outside is sent towards it based on a quadratic Wendland function

$$s(\boldsymbol{x}) = \Pi\left(1 - \frac{\frac{||\overrightarrow{\boldsymbol{px}}||}{\Pi} - 1}{\sigma}\right)_+^2 \qquad \text{for } ||\overrightarrow{\boldsymbol{px}}|| > \Pi, \tag{4}$$

where $\boldsymbol{x} \in \Omega_{I_\alpha}$ and $(\cdot)_+ = \max(\cdot, 0)$. The effects of Π and σ are illustrated in Fig. 3. It can be shown that s is invertible w.r.t. every $\boldsymbol{y} \neq \boldsymbol{p}$ by solving the quadratic equation

$$-\frac{1}{\sigma^2}\left(\frac{||\overrightarrow{\boldsymbol{px}}||}{\Pi}\right)_x^2 + \left(1 + \frac{2}{\sigma} + \frac{2}{\sigma^2}\right)\frac{||\overrightarrow{\boldsymbol{px}}||}{\Pi} + \left(-\frac{1}{\sigma^2} - \frac{2}{\sigma} - 1 - \frac{||\overrightarrow{\boldsymbol{py}}||}{\Pi}\right) = 0, \tag{5}$$

for $||\overrightarrow{\boldsymbol{px}}||$, such that $s^{-1}(\boldsymbol{y}) = s(\boldsymbol{x})$ for $\boldsymbol{y} = \boldsymbol{x} - s(\boldsymbol{x})\frac{\overrightarrow{\boldsymbol{px}}}{||\overrightarrow{\boldsymbol{px}}||}$ thus resulting in $\boldsymbol{x} = \boldsymbol{y} + s^{-1}(\boldsymbol{y})\frac{\overrightarrow{\boldsymbol{py}}}{||\overrightarrow{\boldsymbol{py}}||}$.

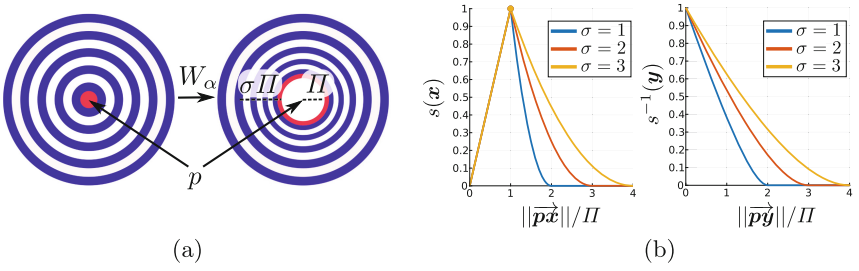

(a) (b)

Fig. 3. (a): Radial point expansion in a toy example with $\sigma = 2$. Note how the compression of the circles increases towards the center of expansion. (b) Scaling of displacement (left) and inverse displacement (right) w.r.t. distance to expansion center p for various σ after factoring out Π.

The line segment extends the model from a discrete point expanding radially to a straight line segment defined by two endpoints $\boldsymbol{p_0}$ and $\boldsymbol{p_1}$ expanding primarily along its normal directions and semi-radially at its endpoints. For a

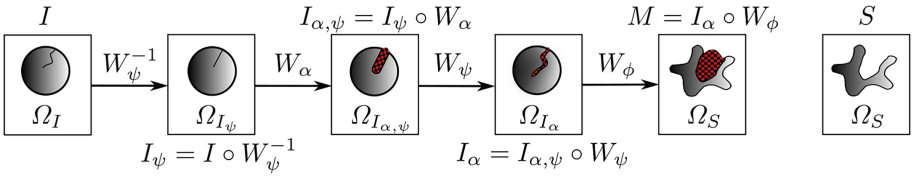

Fig. 4. The curved discontinuity is straightened from Ω_I to Ω_{I_ψ}, and its topology is then altered when moving to $\Omega_{I_{\psi,\alpha}}$. The curvature is then reintroduced going back to Ω_{I_α} where we apply W_ϕ as usual.

given $\boldsymbol{x} \in \boldsymbol{\Omega_{I_\alpha}}$, let $\boldsymbol{p}$ be the closest point on the segment $\overrightarrow{\boldsymbol{p_0 p_1}}$, which is readily found by vector projection. The expansion is again modeled by a radius Π such that any $\boldsymbol{x}$ with $||\overrightarrow{\boldsymbol{px}}|| < \Pi$ is within the resulting hole, and the displacement is computed in the same way as for the sphere.

The quadrilateral extends the concept to expansion from a parallelogram in 3D. The discontinuity consists of all points contained in the parallelogram given by the corners $\boldsymbol{p_0}, \boldsymbol{p_1}, \boldsymbol{p_2}$ and $\boldsymbol{p_0} + \overrightarrow{\boldsymbol{p_0 p_1}} + \overrightarrow{\boldsymbol{p_0 p_2}}$. Given a point $\boldsymbol{x}$, we again find the closest point $\boldsymbol{p}$ in the discontinuity through vector projection, and determine the expansion as usual.

Curvature. The line segment and quadrilateral discontinuities assume the discontinuities in the source to be straight, which is seldom the case. However, any curved line segment or quadrilateral is diffeomorphic to its straight counterpart. Consider a curved discontinuity in Ω_I and let $W_\psi \colon \Omega_I \to \Omega_{I_\psi}$ be a diffeomorphism altering I to get a straight discontinuity in $I_\psi = I \circ W_\psi^{-1}$. We thus compute the change-of-topology in Ω_{I_ψ} with the usual model and return the result to Ω_{I_α} as shown in Fig. 4 (extending Fig. 2). As W_ψ only depends on the initial shape of the discontinuity in I it only needs to be computed once.

3 Experiments and Results

Our model is implemented for GPU processing using C++ and CUDA. The diffeomorphic model (TopAwaRe_D) controlling W_ϕ is based on LDDMM [3] and optimizes the normalized cross-correlation (as in [1]) over a time-dependent velocity field. The whole warp is optimized in a multi-scale scheme.

We validate our models via intersubject registration of T1-weighted MRI 3D brain volumes from the MICCAI2012 [7] database, which contains 32 subjects with 139 expert-labeled anatomical regions. From these, we identify 6 subjects of interest (SOI) with particularly expanded ventricles in the back, which cannot be registered correctly to a normal subject using diffeomorphic registration, as global continuity leads to an incorrect stretching of subcortical regions in order to map a normal ventricle to an expanded one (see Figs. 5 and 7). The results are thus divided into pairwise registrations between all 32 subjects ($N = 992$)

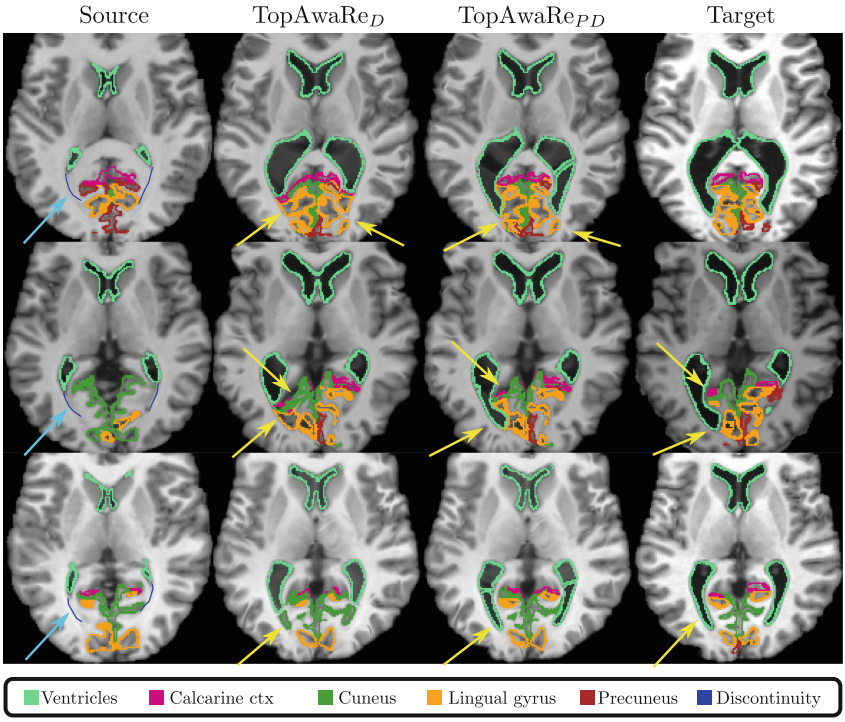

Fig. 5. Registration from sources with contracted ventricles to expanded targets. The topological changes causes clear issues in their neighbourhoods. Blue arrows emphasize delineated discontinuities and yellow arrows point to subcortical regions incorrectly registered by the diffeomorphic model. (Color figure online)

and normal subjects to SOI ($N = 156$). All subjects are affinely preregistered to a common space of size $182 \times 218 \times 182$ voxels.

To facilitate TopAwaRe$_{\text{PD}}$, the two contracted ventricles of a single normal subject were manually delineated by 25 control points each. This subject was then registered to the rest and the control points coregistered accordingly to automatically obtain a discontinuity surface per source image (shown in Fig. 5). The background image β of Eq. (1) was set to a constant value of 0.2, corresponding roughly to the average intensity within the ventricles, such that points within the modeled holes are treated as ventricles when evaluating the results.

Validation of TopAwaRe$_{\text{D}}$: Over all samples, our base diffeomorphic implementation produces comparable results to those of the state-of-the-art ANTs framework [1] in terms of global Dice overlap of the 139 coregistered regions (Fig. 6). We thus conclude that our base model is on the level of the state-of-the-art and therefore a fair benchmark for the piecewise-diffeomorphic TopAwaRe$_{\text{PD}}$.

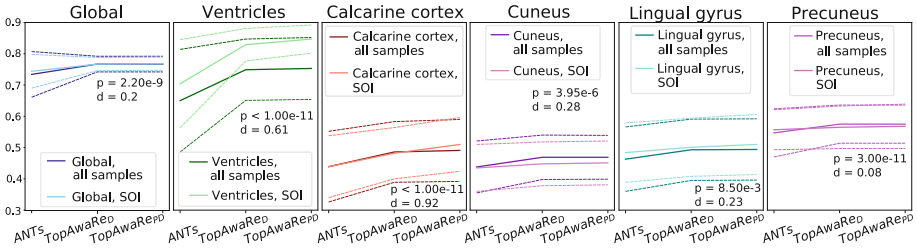

Fig. 6. Mean (solid) and standard deviations (dashed) of Dice overlaps over all samples and SOI. The p- and Cohen's d-values are for the paired t-tests (see below).

Validation of TopAwaRe$_{PD}$: To validate TopAwaRe$_{\mathrm{PD}}$, we investigate the registration of the ventricles as well as four anatomical structures lying between them, both on all samples and the SOI. In Fig. 5 we illustrate a random selection of pairs of normal sources registered to targets with expanded ventricles. As in Fig. 1, the mistakes of the diffeomorphic registrations caused by the topological differences are evident. In particular, subcortical regions near the ventricles are clearly incorrectly registered as emphasized by the yellow arrows.

TopAwaRe$_{\mathrm{PD}}$ captures the topological differences by modeling the ventricle expansions by growing new matter between the touching boundaries of a normal ventricle, and consequently prevents incorrect stretching of adjacent regions. These observations are supported by the Dice overlaps as presented in Fig. 6. Paired one-sided t-tests were performed on the SOI results for TopAwaRe$_{\mathrm{PD}}$ versus TopAwaRe$_{\mathrm{D}}$. To assess effect size, the p-values were supplemented by the corresponding Cohen's d (see p- and d-values in Fig. 6). With significance level 0.05 (Bonferroni corrected threshold 8.33e-3 for 6 tests) we obtain statistically significant improvement in all but the Lingual gyrus region which fails marginally. To further illustrate the differences, in Fig. 7 we show an example of a registration of a healthy control to an Alzheimer's patient from ADNI [8]. The

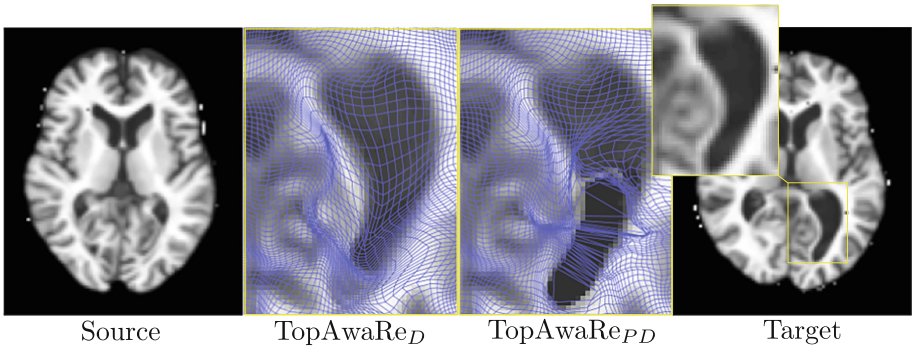

Fig. 7. Example registration from healthy subject to Alzheimer's patient shown with warp grids in selected region. Note: the grids are best viewed on a digital display.

diffeomorphic model stretches an open ventricle to match a large cavity while the piecewise-diffeomorphism opens a contracted ventricle. The warp grid shows how both the ventricle and surrounding tissue are affected by the diffeomorphic model's stretch similar to the effects on subcortical regions seen in Fig. 5.

4 Discussion and Conclusion

We have presented a novel framework for piecewise-diffeomorphic registration, preventing gross local misregistration caused by topological inconsistencies by applying knowledge of the underlying matter's topology. The model has been applied to a diverse dataset, showing that the piecewise-diffeomorphism can be used to prevent incorrect registration at and nearby certain topological differences. In particular, we show improvement in the face of expanded ventricles; a known side-effect of pathological conditions such as Alzheimer's disease.

The standard global Dice overlap is well suited to show that our diffeomorphic base model TopAwaRe_D performs comparably to ANTs [1], but is less sensitive to improvements in the small subcortical regions shown in Fig. 5. Even the region-wise Dice overlap is insensitive to local changes if the majority of the region is not near the topological change. The improvements are, however, clear both from selected region-wise Dice coefficients and by visual inspection.

Our model depends on predefined discontinuities. Allowing discontinuities to occur anywhere may result in implausible warping but manual interaction may be costly. In our experiments it sufficed to manually delineate the collapsed ventricles of a single subject and coregister them to other subjects. This indicates some robustness towards the exact location and curvature of the discontinuities.

In its presented form, the framework is not symmetric. Specifically, the topology-altering model allows expansion from discontinuities in the source image but not vice-versa. This could be achieved by applying the model in both directions alongside a symmetric registration model [1].

One might expect the piecewise-diffeomorphic model to incur significant additional computational cost. However, as the size of an expansion is optimized by numerically estimating the gradient w.r.t. a single parameter, the increased cost is modest and the GPU implementation allows fast registration regardlessly.

The current practice in image registration is to accept the incorrect diffeomorphic assumption as unavoidable. We believe that, through additional specialization our model may provide a practical foundation for further improving registration of pathological tissue. We thus hope this might spark interest in the community to move beyond diffeomorphic image registration.

Acknowledgements. This research was supported by the Lundbeck Foundation and by the Centre for Stochastic Geometry and Advanced Bioimaging, funded by a grant from the Villum Foundation.

References

1. Avants, B.B., Epstein, C.L., Grossman, M., Gee, J.C.: Symmetric Diffeomorphic image registration with cross-correlation: evaluating automated labeling of elderly and neurodegenerative brain. Med. Image Anal. **12**(1), 26–41 (2008)
2. Balakrishnan, G., Zhao, A., Sabuncu, M.R., Guttag, J., Dalca, A.V.: An unsupervised learning model for deformable medical image registration. In: Conference on Computer Vision and Pattern Recognition (CVPR), pp. 9252–9260(2018)
3. Beg, M.F., Miller, M.I., Trouvé, A., Younes, L.: Computing large deformation metric mappings via geodesic flows of diffeomorphisms. Int. J. Comput. Vis. **61**(2), 139–157 (2005)
4. Berendsen, F.F., Kotte, A.N.T.J., Viergever, M.A., Pluim, J.P.W.: Registration of organs with sliding interfaces and changing topologies. In: SPIE, vol. 9034, pp. 90340E–90340E-7 (2014)
5. Delmon, V., Rit, S., Pinho, R., Sarrut, D.: Registration of sliding objects using direction dependent B-splines decomposition. Phys. Med. Biol. **58**(5), 1303 (2013)
6. Kwon, D., Niethammer, M., Akbari, H., Bilello, M., Davatzikos, C., Pohl, K.M.: PORTR: pre-operative and post-recurrence brain tumor registration. IEEE TMI (3), 651–667
7. Landman, B.A., et al.: MICCAI 2012 Workshop on Multi-Atlas Labeling. CreateSpace, Scotts Valley (2012)
8. Mueller, S.G., et al.: Ways toward an early diagnosis in Alzheimer's disease: the Alzheimer's disease neuroimaging initiative (ADNI). Alzheimer's Dement. **1**(1), 55–66 (2005)
9. Papież, B.W., Heinrich, M.P., Fehrenbach, J., Risser, L., Schnabel, J.A.: An implicit sliding-motion preserving regularisation via bilateral filtering for deformable image registration. Med. Image Anal. **18**(8), 1299–1311 (2014)
10. Risser, L., Baluwala, H.Y., Schnabel, J.A., Vialard, F.X.: Piecewise-diffeomorphic image registration: application to the motion estimation between 3D CT lung images with sliding conditions. Med. Image Anal. **17**(2), 182–193 (2012)